RSC Advances

ROYAL SOCIETY OF CHEMISTRY

www.rsc.org/advances

Study on the Photophysical and Electrochemical Property and Molecular Simulation of Broadly Absorbing and emitting Perylene Diimide Derivatives with Large D-π-A structure

Long Yang [a], Yuyan Yu [a], Jin Zhang [a], Yuanqing Song [a], Long Jiang [a], Fang Gao [b] and Yi Dan [*a]

Abstract: To obtain broadly absorbing perylene derivatives with the synchronous impact of intrinsic π-π* transition of large conjugated system and intra-molecular charge transfer (ICT), we report here the facile synthesis and physical characterization of new type N-(n-octylaminyl)-3,4,9,10-perylene tetracarboxylic acid diimides (PDI) bearing benzyl substituted quinoline-4(1H)-ylidene-methyl unit as effective donors on the 1,7-position (**C1**) and 1-position (**C2**). Compared to unsubstituted PDI, **C1** and **C2** both show a pronounced bathochromic shift to the near infra-red region, high molar extinction coefficient, concentration-dependent π-π stacking induced fluorescence and low LUMO energy level. The investigation of spectroscopic properties and molecular simulation reveals effective ICT character in compounds **C1** and **C2**. All the properties and analysis indicate that the derivatives are efficient solar-harvesting and potential candidate materials for the use in photovoltaic devices and photo-catalyst.

Keywords: perylene diimide, donor-π-acceptor, broad absorption, π-π stacking, intra-molecular charge transfer (ICT).

Introduction

To make full use of solar energy in the aspects of renewable energy sources and construction of solar energy conversion systems, many research efforts have been focused on the exploration of molecular photoelectric devices in photochemical energy conversion, which requires high light harvesting and electron transporting capacity and excellent photo-induced intra-molecular charge transfer (ICT). For this purpose, recent developments in the fields of organic photovoltaics have boosted great interest in the design of an innovative class of photo-functional polymers and dyes or pigments exhibiting broad light harvesting range in the visible and near-infrared (NIR) region to attain more efficient solar energy.[1] The unavoidable shortcoming of the used materials is highly cost. Accordingly, dyes or polymers with facile modification synthetic route will be in huge demand. At the mean time, materials with lower LUMO energy level will facilitates the electron transporting in hybrid materials [2] or from the light harvesting unit to the conducting band of semiconductor (i.e. TiO_2, ZnO_2) [3].

Perylene diimides (PDI), a class of industrial dyes which represent highly chemistry, photo and thermo-stable n-type semiconductors [4] with relatively good electron affinity, high molar extinction coefficient and excellent transport property are potential candidates as electron-accepting materials in many aspects such as organic photovoltaic solar cells [5], light-harvesting arrays [6], organic-polymer hybrid material [7] and the photo-induced energy and electron-transfer process [8]. Moreover, high electron mobility through π-π stacking favors ICT and increases the charge separation. [9] In this regard, the selection of a suitable donor-π-acceptor (D-π-A) structure with large conjugated system is the most important parameter to achieve the above goals.

Extending the intrinsic light absorption range (400 - 550 nm) of PDI,[10] the substitution in the bay region of PDI through C-C or C-N coupling is a simple route to modify the HOMO-LUMO level renders to extend the visible - NIR absorption region of the derivatives as compared to unsubstituted PDI. [11] The former methods consumed several synthetic steps with high cost and the absorption of some derivatives could not cover the whole visible - NIR range. And at the mean time, the introduction of strong electron donating substituent which enhances the ICT effect unfavorably increases the LUMO energy level [12] and unfortunately high LUMO level will not favor charge transfer process [13].

Thus a new idea is put forward by introducing a conjugated substituent without perturbing the electronic transition of perylene ring extremely, the synchronous impact of π-π* transition absorption of large conjugated system and ICT transition absorption can broaden the visible-NIR absorption without significantly increasing the LUMO energy level. Additionally, recent studies revealed that the presence of a quinoidal fragment in the molecules of NIR absorption dyes led to significant bathochromic shift of their absorption.[14] To verify the proposition and obtain visible-NIR absorbing light-harvesting sensitizers and materials with large D-π-A structure, under the above guideline target compounds with merocyanine substituent through C=C bond will be introduced on the bay region of perylene ring with quinoidal push-pull structure and the diimide moiety as the acceptor. Heavy atom Br will be introduced as a medium electron-withdrawing substituent to demonstrate the effect on LUMO energy [15] and the effect on the aggregation behavior and for comparison the strong donor (n-octylamine) substituted perylene derivative (**C3**) will also be synthesized and investigated.

Herein, a simple synthetic method will be applied to obtain perylene derivatives with large D-π-A system, light absorption covering the range of 400 - 750 nm and low LUMO energy. In addition to the research of photo absorption property, the unusual fluorescence emission, electrochemical properties and molecular modeling will also be investigated and discussed.

Experiment section

Starting materials

Perylenetetracarboxylic acid anhydride, liquid bromine, n-octylamine and benzyl bromide were purchased from Chengdu Astatech Trading Co., Ltd.. 4-methylquinoline and N-ethyldiisopropylamine were obtained from Suzhou Yacoo corporation and Adamas-beta (Shanghai, China), respectively. All the starting materials and reagents were used without further purification. Column chromatography was performed on silica gel (70-80A, Qingdao Hailang).

Analysis instruments

^{1}HNMR spectra were recorded on a Bruker Avance□-400MHz. UV / vis spectra were recorded on a UV-2300 spectrophotometer (Hitachi, Japan). Fluorescence spectra were recorded on an F4600 spectrometer (Hitachi, Japan) excited at 430 nm for solution and 400nm for thin film. The molecular ground-state geometries were optimized using Becke's three parameter hybrid exchange-correlation (XC) functional B3LYP [16] and 6-31G (d, p) basis which were performed using Gaussian 03 software package [17]. The electrochemical measurements were carried out

on the CIMPS workstation (Zahner Elektrick Co., Germany).

Synthesis and characterization

The chemical structures of target compounds and the synthetic routes used for the preparation were outlined in Figure 1 and Scheme 1. Further synthetic procedures were described as follows.

Br-PDI

Br-PDI was synthesized according to the literature.[18] To a solution of concentrated sulfuric acid (150 mL) was added perylenetetracarboxylic acid anhydride (5.0 g, 12.7 mmol). After stirred for 0.5 h at room temperature, the mixture was warmed to 55 - 60 °C, and iodine (0.3 g, 1.27mmol) was added. After 3 h, bromine (1.7 mL, 31.8 mmol) was added to the mixture slowly which was then warmed to 85 °C and stirred for 8 h. After burbled excess bromine with N_2 gas into aqueous NaOH solution, the mixture was quenched with ice water and filtered under reduced pressure, washed with water, dried under vacuum to give red solid (6.5 g) which was used in the next step directly.

A suspension of brominated perylene dianhydrides (5.0 g, 90.9 mmol) obtained in the above reaction, n-octylamine (3.5 g, 27.1 mmol), and acetic acid (2.5 g, 41.7 mmol) in 50 mL of N-methyl-2-pyrrolidinone was stirred at 85 °C under Ar for 8 h. After cooled to room temperature, the mixture was poured into water, and the precipitate was separated by filtration, washed with 100 mL of MeOH, then dried under vacuum at 40 °C. The crude product was purified by silica gel column chromatography with CH_2Cl_2 : hexane (1:1) as eluent. A mixture of 1,7- and 1,6-dibromoperylene diimide as a red powder was obtained. The regioisomeric 1,7-dibromoperylene diimide (3.2 g, 42.4%) was obtained through two recrystallization procedures. ^{1}H-NMR (400 MHz, $CDCl_3$): δ = 9.420-9.440 (d, J=8.0Hz, 2H), 8.873 (s, 2H), 8.648-8.668 (d, J=8.0Hz, 2H), 4.176-4.214 (t, J=7.6Hz, 4H), 1.728-1.762 (m, 4H), 1.252-1.438 (m, 20H), 0.865-0.898 (t, J=6.6Hz, 6H).

QL

The reaction mixture of 4-methylquinoline (5.0 g, 34.5 mmol) and benzyl bromide (11.8 g, 69.0 mmol) was heated to reflux for 3.0 h. After cooled to room temperature, the mixture was poured into absolute ether, and the formed precipitate was separated by filtration, washed and dried under vacuum to give light gray solid (9.8 g, 89.9%) which was used directly in the next step.

C1 and C2

C1 and **C2** were synthesized according to the literature.[19] Br-PDI (0.50 g, 0.65 mmol) and the quaternary intermediates QL (0.41 g, 1.30 mmol) were dissolved in 15 mL of NMP in a Schlenk flask and were flushed with argon. The reaction mixture was heated to 115 °C and a mixture of N-ethyldiisopropylamine (0.50 g, 3.90 mmol)and pyridine (0.62 g, 7.80 mmol) was added rapidly. After 45 minutes at this temperature, the reaction mixture was cooled to room temperature and poured into 150 mL of a 3:1 mixture of distilled water/acetone. The formed precipitate was suction filtered, washed with water, and dried under vacuum. The crude product was further separated through column chromatography on silica gel (methylene chloride/hexane = 3:1) to give **C1** (dark purple solid, 0.30 g, 43%) and **C2** (dark red solid, 0.15 g, 25%).

C1, ^{1}H-NMR (400 MHz, $CDCl_3$): δ = 8.501-8.576 (m, 2H), 8.353-8.370 (d, J=6.8Hz, 2H), 7.393-7.430 (t, J=7.4Hz, 5H), 7.283-7.352 (m, 8H), 7.152-7.229 (m, 1H), 7.033-7.110 (m, 2H), 6.685-6.811 (m, 4H),4.755-4.838 (m, 6H), 4.038-4.131 (m, 4H), 3.942-3.997 (dd, J=6.4Hz, 2H), 3.737-3.794 (dd, J=6.0Hz, 2H), 1.660-1.693 (m, 4H), 1.257-1.390 (m, 20H), 0.846-0.863 (m, 6H).

C2, ^{1}H-NMR (400 MHz, $CDCl_3$): δ = 8.547-8.615 (m, 4H), 8.383 (s, 1H), 7.384-7.421 (t, J=7.4Hz, 2H), 7.255-7.338 (m, 3H), 7.141-7.159 (d, J=7.2Hz, 1H), 7.046-7.085 (t, J=7.8Hz, 1H), 6.706-6.743 (t, J=7.4Hz, 2H), 6.197-6.216 (d, J=7.6Hz, 1H), 4.746-4.824 (m, 3H), 4.105-4.183 (m, 4H), 3.924-3.966 (d, J=16.8Hz, 1H), 3.711-3.753 (d, J=16.8Hz, 1H), 1.693-1.729 (m, 4H), 1.269-1.427 (m, 20H), 0.832-0.869 (m, 6H).

C3

A suspension of **Br-PDI** (0.20 g, 0.26 mmol), n-octylamine (0.02 g, 0.13 mmol) and pyridine of catalytic amount in NMP (10.0 ml) was vigorously stirred and heated at 70°C under argon for 1 h. After being cooled to room temperature, the reaction mixture was added to water (50.0 ml) slowly. The resulting green precipitate was filtered off and repeatedly washed with water and methanol. After dried under vacuum, the crude product was purified by column chromatography on silica gel (methylene chloride) to give **C3** (0.11 g, 87.1%) as dark green powder. ^{1}H-NMR (400 MHz, $CDCl_3$): δ = 8.660-8.680 (d, J=8.0Hz, 1H), 8.432-8.452 (d, J=8.0Hz, 1H), 8.317-8.337 (d, J=8.0Hz, 1H), 8.200-8.220 (d, J=8.0Hz, 1H), 8.114-8.135 (d, J=8.0Hz, 1H), 8.026-8.046 (d, J=8.0Hz, 1H), 5.932 (s, 1H), 4.137-4.173 (t, J=7.2Hz, 4H), 3.426-3.453 (t, J=5.4Hz, 2H), 1.835-1.870 (m, 2H), 1.735-1.769 (m, 4H), 1.318-1.622 (m, 30H), 0.87-0.93 (m, 9H) .

Results and discussion

Photophysical properties - Absorption

The steady-state UV-visible spectra of **C1**, **C2** and **C3** were recorded in 1.0×10^{-5} M solutions in $CHCl_3$ (Figure 2). The perylene derivatives all have broad absorption in visible light range from 400 to 750 nm. **C1** and **C2** both exhibit typical π - π* transition in the range of 400 - 580 nm ($S_0 \rightarrow S_1$ transition) [20] with well resolved vibronic structure that can be attributed to breathing vibrations of the perylene skeleton whereas the relative breathing vibrations in compound **C3** is perturbed by the amine group which results in the red-shift of broad absorption in 520 - 750 nm region. The higher energetic $S_0 \rightarrow S_2$ transition is also observed at absorption maxima around 385 nm (for **C1** and **C2**) and 429 nm (for **C3**) [21]. Due to larger conjugated degree (44 aromatic electrons for **C1** and 32 aromatic electrons for **C2**) caused by C=C bonds connected quinoline moiety, within 400 - 580 nm range the absorption maxima appears to be apparent red-shift for **C1** (30 nm) and **C2** (20 nm) comparing to bay un-substituted perylene derivatives [22]. Additionally, the target compounds present obvious long-wavelength absorption with ICT characteristic in the range of 580 - 750 nm ($S_0 \rightarrow S_1$ transition) which confirms effective charge transfer between the donor (merocyanine part) and acceptor (perylene diimide part). Notably, the breathing vibrations of the perylene skeleton of **C1** and **C2** are not perturbed by the ICT effect and the quinoidal structure substituent group which results in broad absorption with high molar extinction coefficient (Table 1).

Table 1 Absorption properties of **C1**-**C3** in $CHCl_3$ solution (1.0×10^{-5} M)

Compound	Absorption				Energy gap
	λ_{max} (nm) / 10^5 ε (L / mol $^{-1}$ cm $^{-1}$)				λ_{onset}(nm) / E_{gap} [a] (eV)
C1	-	520.8 / 0.26	559.6 / 0.38	627.6 / 0.10	760 / 1.632
C2	474.5 / 0.15	505.3 / 0.30	545.7 / 0.68	621.8 / 0.06	758 / 1.636
C3	428.6 / 0.16	-	-	626.1 / 0.24	745 / 1.664

[a] $E_{gap} = 1240 / \lambda_{onset}$.

Additionally, UV-visible spectra of **C1**, **C2** and **C3** were recorded at different concentrations (0.05×10^{-5} to 10.0×10^{-5} M) in $CHCl_3$ in order to understand the aggregation properties of the perylene diimide derivatives (Figure 3). In the visible-NIR range, the intensity of π - π* vibronic transitions and ICT absorption for the whole range of concentrations (0.5×10 - 5 to 5.0×10^{-5} M) both do not vary considerably, whereas at the concentrated solution (10.0×10^{-5} M) the absorption peaks and intensity of vibronic transitions both change dramatically. Thus, aggregation effect can be excluded at concentrations up to 5.0×10^{-5} M according to the photo-absorption property. Consequently, absorption and photoluminescence measurements will not be perturbed by aggregation between molecules in dilute solutions in a measurement range up to this concentration.

The frontier orbital HOMO-LUMO energy gap (Egap) was determined from the UV-visible absorption spectra [23] (Table 1). The E_{gap} of **C1** (1.632 eV) and **C2** (1.636 eV) are slight lower than that of **C3** (1.664 eV) due to much larger degree of conjugated system in **C1** and **C2** which also results in obvious red-shift of the absorption maxima of the perylene skeleton (Figure 2).

Photophysical properties - Emission

To study the excited state property, fluorescence spectra (Figure 4) of **C1**, **C2** and **C3** were recorded in $CHCl_3$ solution and all the samples were selectively excited at 430 nm (The select of excitation wavelength in the visible light range was based on the exclusion of frequency peak interference with the emission peak.) in the same condition . In Figure 4b, at the concentration of 5.0×10^{-5} M the derivatives all exhibit broad emission in the range of 450-850 nm, among which 450 - 650 nm range belongs to the radiation of the excited state of perylene skeleton, while 650 - 850 nm range belongs to the ICT ($S_1 \rightarrow S_0$ transition) characteristic. Remarkably, the heavy atom (Br) in **C2** and **C3** does not play a dominant role in the change of emission peaks (Table 2). The emission maxima in the wavelength range of 450 - 650 nm increase in the order of **C3** → **C2** → **C1** which can be attributed to the increase of conjugated degree of perylene ring with merocyanine substituent. Whereas the ICT emission peak exhibits in the order of **C3** > (**C1** and **C2**), mainly because the lone electrons of amine substituent offer isolated electrons and extremely enhances ICT content between the donor (amine group) and acceptor (diimide moiety) (Figure 5).

Table 2 Emission properties of **C1**-**C3** in $CHCl_3$ solution (5.0×10^{-5} mol/L)

Compound	λ_{max} (nm)				ICT Stokes shift (nm)
C1	484	532	585	719	92
C2	481	529	576	715	93
C3	481	515	-	723	97

Notably, the derivative **C1** exhibits obvious intensity and peak change of emission (Figure 4a) in the long-wavelength (650 - 850 nm) range at different concentrations which can be attributed to effective charge transfer between the Donor (merocyanine part) and acceptor (perylene diimide part) (ICT emission peak). As concretely illuminated in depth in Figure 6, with the increase of concentrations of dilute solution from 0.6×10^{-5} M to 5.0×10^{-5} M, the intensity slightly increase and the emission maxima appears slight change. When the concentration increases up to 1.0×10^{-4} M, the emission maxima presents apparent red-shift, and in the concentration of 5.0×10^{-4} M the intensity decreases and the emission maxima presents dramatic red-shift indicating the emergency of inter-molecules action which consequently results in the absence of the emission peak of short-wavelength range (450 - 650nm) due to strong π-π interaction of the perylene rings upon aggregation [24]. This is a remarkable result, because aggregation often opens up new pathways for quenching of the excitation energy; this can be observed for many extended π systems, including many perylene derivatives in the solid state [25]. Similar critical concentration (1.0×10^{-4} M) of apparent intermolecular action can be drawn from fluorescence spectra compared with UV-visible absorption spectra (5.0×10^{-4} M).

To study systematically the aggregation behavior of fluorescence emission, the concentration dependant intensity changes of each emission peak in the range of 450 - 850 nm are drawn in Figure 7. Upon the concentration of **C1** in $CHCl_3$, the intensity of emission peaks (W1, W2, W3 and W4) all increase normally until a critical concentration at which the probability of intermolecular action and the effect of fluorescence quenching increase. Notably, upon the concentration increases to 5.0×10^{-4} M, the fluorescence intensity of ICT emission peak exhibits higher than that of short-wavelength emission of perylene skeleton. Remarkably, the ICT emission peak keeps the shape with a slight shoulder peak on the right and no new long-wavelength emission is observed, hence the emission of excimer is excluded. The same results have also been obtained for **C2** and **C3**. This phenomenon could be attributed to π-π stacking induced quenching of short-wavelength emission and enhancement of ICT character emission due to the disappearance of short-wavelength emission peak (W2, W3 and W4).

To investigate further the aggregation induced photophysical behavior of the derivatives in solid state, the UV-visible absorption spectra and fluorescence spectra (Figure 8) were performed on quartz glass on which thin films were obtained through dip-evaporation. **C1**, **C2** and **C3** all show broad absorption from 400 nm to 900 nm which make the derivatives be well suitable for light-harvesting materials. The disappearance of well resolved vibronic absorption structure can be attributed to the aggregation of ground-state molecules through the stacking of π-π conjugated plane which was further verified through the disappearance of the 500 - 650 nm emission peaks in solid state on quartz glass. The strong π-π interactions also lead to an almost complete loss of fine structure of fluorescence emission. Interestingly, compared with the fluorescence behavior in $CHCl_3$ solution, the 750nm ICT emission peak extremely decreases.

The 800 - 850 nm emission peak might be assigned to frequency peak of the excitation light. To gain more information about the aggregation behavior of the derivatives with large π conjugation system, the self-assembly property will be carried out in the next research focus.

The Stokes shift is defined as the difference between the absorption and emission maxima which can be used to evaluate the non-radiative energy loss in the excited state. The ICT absorption and emission of the three derivatives all exhibit large Stokes shift: 92 nm (**C1**), 93 nm (**C2**) and 97 nm (**C3**) (Table 1 and 2, Figure 9) corresponding 2025 cm^{-1}, 2096 cm^{-1} and 2140 cm^{-1} in wavenumbers, respectively. The large Stokes shift also indicates the effective ICT character of **C1** and **C2** and non-radiative energy loss which could be partially explained with large dihedral angles between the acceptor (perylene ring) and the donor (quinoline moiety) in the ground state (See computational analysis).

Computational Analysis

In order to support and clarify the experimental results further, theoretical calculations on the molecules were performed to gain deeper insight into the optimized structure, the electric properties and the electron-density distribution of the frontier orbital.

Table 3 The molecular structure property of **C1**-**C3** calculated by DFT calculation (in vacuum)

Compound	Dipole (D)	HOMO (eV)	LUMO (eV)	E_{gap} (eV)	Dihedral (°)	
					D_1	D_2
C1	6.79	- 4.52	- 2.86	1.66	18.15	38.05/40.76
C2	9.30	- 4.91	- 3.14	1.77	18.33	36.53
C3	4.73	- 5.54	- 3.25	2.29	18.31	10.78

The dipole moments (Table 3) calculated by DFT method in the ground state are 6.79 D (**C1**), 9.30 D (**C2**) and 4.73 D (**C3**). The large values indicate the strong asymmetric distribution of positive charge and negative charge and the potentiality of the derivatives. The dipole moments of **C1** and **C2** are highly larger than that of C3, thus

reasonably the ICT character of **C1** and **C2** is much stronger. Through geometry optimization, the non-planarity of the perylene core is discovered, and the dihedral angles of perylene core (18.15° for **C1**, 18.33° for **C2** and 18.31° for **C3**) (Table 3 and Figure 10) of **C2** and **C3** are within the dihedral angle range of common perylene diimide derivatives (0-38°). Remarkably, the small dihedral twist angles of **C1**, **C2** and **C3** reveal the concentration-dependant unusual fluorescence induced by molecular aggregation.[26] The dihedral angles between the perylene ring and quinoline moiety for **C1** (38.05° and 40.76°) and **C2** (36.53°), amine substituent and perylene ring for **C3** (10.78°) are also given.

The ICT effect can also be elucidated through the electron density of the highest occupied molecular orbital (HOMO) and lowest unoccupied molecular orbital (LUMO). For **C1** and **C2**, the HOMO is mainly located on the quinoline moiety whereas the LUMO is more spread over the perylene region, representing for large degree of intra-molecular charge transfer in the ground state. However, for **C3** the HOMO and LUMO are both mainly located on the perylene ring.

As clearly showed in Table 3, the calculated HOMO and LUMO energy levels in the ground-state optimized geometry are found to be - 4.52 eV and - 2.86 eV for C1, -4.91 eV and -3.14 eV for C2 and -5.54 eV and -3.25 eV for C3, respectively, which are in good agreement with the electrochemically determined HOMO and LUMO energy levels (Table 4). Comparing the HOMO energy levels, the increase of the values (- 4.52 eV > - 4.91 eV > -5.54 eV) could be assigned to the larger degree of π-conjugation system spreading over perylene ring and the quinoline moiety and the electron-donating effect of the nitrogen in the quinoline moiety as showed in the electron-density distribution of HOMO. In contrast, the incorporation of electron-withdrawing substituent (Br) fails to significantly lower the LUMO energy levels. The increase of HOMO energy level and decrease of LUMO energy level effectively lead to relatively narrow band gap of **C1** (1.66 eV) which is in good accordance with the value determined from λ_{onset} of UV-vis absorption spectra . A conclusion can be drawn that the incorporation of quinoline substituent through C=C bond can effectively extend the π conjugated system, enhance the ICT extent, and accordingly narrow the band gap and broaden the photo absorption range without significantly perturbing the vibronic transition of perylene skeleton.

With the initial and bold attention to understand the unusual emission peak, the electronic structures of frontier orbital of **C1** are also discussed. Figure 12 shows the electron density distribution and energy levels of the frontier molecular orbital (HOMO-2, HOMO-1, HOMO, LUMO, LUMO+1 and LUMO+2) of **C1**. As the same as HOMO, the electron density of HOMO-1 is spread over the whole conjugated system, while HOMO-2 is predominantly located on the perylene skeleton, respectively. On the other hand, the electron density of LUMO+1 is located on the perylene ring, while LUMO+2 is spread mainly over one side of whole conjugated system. The E_{gap} of HOMO-1 ~ LUMO, HOMO-2 ~ LUMO, HOMO ~ LUMO+1 and HOMO ~ LUMO+2 are 2.09 eV, 2.80 eV, 3.10 eV and 3.12 eV, respectively. The λ_{onset} of the 560 nm absorption peak is about 580 nm (2.13 eV) which is well matched with the Egap of HOMO-1 ~ LUMO transition. Thus supported by the former research, [27] we predict that the electric transition corresponding to the absorption peak of 560 nm mainly originates from the excitation from HOMO-1 to LUMO. Moreover, the electric transition of HOMO-1 ~ LUMO, HOMO-2 ~ LUMO, HOMO ~ LUMO+1 and HOMO ~ LUMO+2 all exhibit ICT character to some extent and this behavior might be another factor that causes the red-shift of the absorption maxima of perylene skeleton. Remarkably, as the concentration would have significant influence on the ICT behavior, the electric transition HOMO-1 ~ LUMO, HOMO-2 ~ LUMO, HOMO ~ LUMO+1 and HOMO ~ LUMO+2 with ICT character may be another factor that results in the unusual change of fluorescence emission of the W2 - W4 peaks at concentrated solutions as elucidated in the fluorescence analysis .

Cyclic voltammograms

Further insight into the electronic properties of the perylene derivatives was gained by Cyclic voltammetry. The experiments were performed in a three-electrode system using platinum plate as working electrode and Ag / $AgNO_3$ as reference electrode in acetonitrile solvent containing 0.1M n-Bu_4NPF_6 as conducting electrolyte at a scan rate of 100 mV . s^{-1}. The samples were dissolved in acetonitrile solution (1.0×10^{-4} M) . The solutions were purged with argon for 25 min before each measurement. All potentials were internally referenced to the Fc (ferrocene) / Fc^+ couple. [28]

Table 4 Electrochemical properties and the estimated MO energies of the perylene derivatives with respect to the vacuum level

Comp.	E_{ox} /V	E_{red} /V	HOMO (eV)	LUMO (eV)	E_{gap} (eV)
C1	- 1.10, - 0.94, 0.49	- 1.24, - 1.00	- 5.29	- 3.80	1.49
C2	- 1.05, - 0.84, 0.53	- 1.23, - 0.97	- 5.33	- 3.83	1.50
C3	- 1.14, - 0.98, 0.47	- 1.09	- 5.27	- 3.71	1.56

$E_{HOMO} = -(E_{onset.ox} + 4.8)$, $E_{LUMO} = -(E_{onset.red} + 4.8)$. [29]

For **C1** and **C2**, the cyclic voltammograms (Table 4 and Figure 13) show two characteristic oxidation and reduction potentials between - 0.7 to - 1.4 V which corresponds to reduction of perylene diimide to dianionic species.[30] Concretely, **C1**, **C2** and **C3** show irreversible oxidation potential at 0.49 V, 0.53V and 0.47 V which imply the oxidation of the substituents moiety (quinoline part for **C1** and **C2**, alkyl amine part for **C3**, respectively) by which HOMO is mainly contributed, while the reversible redox cycle between - 0.7 to - 1.4 V representing for the electrochemical reaction of diimide moiety on which LUMO is mainly located for **C1** and **C2**. Thus the ICT character of the three derivatives is verified through electrochemical property.

The decrease in electrochemical band gap is obtained through the introduction of electron donating and accepting groups at the bay region of PDI. Commonly accepted, the alteration in the HOMO level depends on the oxidation potential of the donating substituent, while the LUMO level is perturbed by the reduction potential of the accepting substituent. As the HOMO and LUMO both have a node on the nitrogen atom of the imide, the nitrogen substituent on the diimide part has little effect on the photophysical behavior and LUMO energy level. Therefore, the change of HOMO and LUMO energy level should be attributed to the introduction of quinoline moiety for **C1** and **C2**. Notably LUMO is partially located on the quinoline group (Figure 11), thus the decrease of LUMO energy level of **C1** and **C2** can be well explained. Moreover, the LUMO of **C2** (- 3.83 eV) is slightly lower than that of **C1** (- 3.80 eV), thus the introduction of heavy atom Br has minor impact on the LUMO energy level. However, compared with **C2** (- 5.33 eV), the increase of HOMO for **C1** (- 5.29 eV) can be attributed to the improvement of conjugated content while the increase of HOMO for **C3** (- 5.27 eV) can be explained by the introduction of isolated p electrons on nitrogen atom of n-octylamine substituent.

For **C1** and **C2**, the electrochemical band gaps (E_{gap}) are calculated as 1.49 eV and 1.50 eV respectively, which are lower than any other PDI derivatives of the same type within our range of knowledge. At the mean time, the band gaps (E_{gap}) calculated through oxidation and reduction potentials are very closed to the values obtained from optical absorption spectra (Table 4) and DFT calculation (Table 3). But for **C3**, the band gap (2.29 eV) calculated through molecular model is higher than the valves obtained from optical absorption spectra (1.66 eV) and cyclic voltammetry (1.56 eV).

It is believed that the suitable HOMO and LUMO energy level of the organic-polymer hybrid material would be -5.4 eV and -3.9 eV respectively.[31] Moreover, the electron affinity with a LUMO energy level around - 3.8 eV (similar to the LUMO level of widely used PCBM [32] and polymer acceptor on alternating dithienothiophene and perylene diimide units [33]) can facilitate electron acceptor for the use in polymer bulk heterojunction device. Accordingly, **C1** and **C2** are the promising materials replacing PCBM used for further increasing photovoltaic performance together with the excellent characteristics of broad solar light absorption and ICT. Moreover, when used as a donor for efficient bulk heterojuction solar cells utilizing PCBM as the electron acceptor, the energy levels of **C1** and **C2** fit very well with the required energy levels (E_{HOMO} level between 5.2 - 5.8 eV; E_{LUMO} level between 3.8 - 4.0 eV).[34] Taking into account a LUMO energy level for PCBM at - 4.3 eV and using semi-empirical estimation equation,[35] the calculated open circuit voltage (V_{oc}) is ca. 0.69 V for **C1** and 0.73 V for **C2**, respectively, which are close to the data obtained from poly (2,7-carbazole-DPP) derivative as the donor [36].

Conclusion

In summary, merocyanine substituted D-π-A structural perylene derivatives with large π conjugated system (44 aromatic electrons for **C1**) were synthesized through a simple synthetic method and investigated using UV–visible and fluorescence spectroscopy, cyclic voltammetry and geometry optimization calculation. The effective ICT effect causes the derivatives to owe extended broad absorption with high absorption coefficients within the visible-NIR spectra region and concentration-dependent π-π stacking induced unusual fluorescence emission. Notably, it is a feasible way to extend the solar absorption range with the synchronous impact of intrinsic π-π* transition of large conjugated system and ICT transition. Additionally, the introduction of quinoidal fragment on the bay region results in the low-lying LUMO energy level of **C1** (3.80 eV) and **C2** (3.83 eV) which indicating that the target perylene derivatives are efficient solar-harvesting compounds and an potential candidate material for the use in the photovoltaic device.

Acknowledgements

The authors are grateful to the National Natural Science Foundation of China (Grant nos. 50573052 and 51173116) for supporting this research. We gratefully acknowledge Dr. Xinchao Wang and Yulong Gong (Chongqing University) for the use of Gaussian software packages. We are also indebted to Mr. Fansheng Cheng and Ms. Qun Wang (Chengdu Green Energy and Green Manufacturing Technology R&D Center) for the opportunity to use the electrochemistry measurement workstation.

Notes and References

[a] *State Key Laboratory of Polymer Materials Engineering of China, Polymer Research Institute, Sichuan University, Chengdu 610065, China*
[b] *College of Chemistry and Chemical Engineering, Chongqing University, Chongqing 400044, China*
[*] *Corresponding author, telephone: +86-28-85407286, fax number: +86-028-85402465, e-mail: danyichenweiwei@163.com*
† Electronic Supplementary Information (ESI) available: ^{1}HNMR spectrum of **Br-PDI**, **C1**, **C2** and **C3**.
See DOI: 10.1039/b000000x/

1 C.-Y. Chen, M.-K. Wang, J.-Y. Li, N. Pootrakulchote, L. Alibabaei, C.-h. Ngoc-le, J. D. Decoppet, J.-H. Tsai, C. Grätzel, C.-G. Wu, S. M. Zakeeruddin, and M. Grätzel, ACS Nano, 2009, **3**, 3103; S.-J. Moon, E. Baranoff, S. M. Zakeeruddin, C.-Y. Yeh, E. W.-G. Diau, M. Grätzel and K. Sivula, Chem. Commun., 2011, **47**, 8244; X. Dang, J. Qi, M. T. Klug, P.-Y. Chen, D. S. Yun, N. X. Fang, P. T. Hammond and A. M. Belcher, Nano Lett., 2013, **13**, 637.
2 E. Ahmed, G. Ren, F. S. Kim, E. C. Hollenbeck and S. A. Jenekhe, Chem. Mater., 2011, **23**, 4563; Y. Zhou, L. Ding, K. Shi, Y.-Z. Dai, N. Ai, J. Wang and J. Pei, Adv. Mater., 2012, **24**, 957; R. Schmidt, J. H. Oh, Y.-S. Sun, M. Deppisch, A.-M. Krause, K. Radacki, H. Braunschweig, M. Könemann, P. Erk, Z. Bao and F. Würthner. J. Am. Chem. Soc., 2009, **131**, 6215; T. Lei, J.-H. Dou, Z.-J. Ma, C.-H. Yao, C.-J. Liu, J.-Y. Wang and J. Pei, J. Am. Chem. Soc., 2012, **134**, 20025.
3 Q. Yan, Z. Luo, K. Cai, Y. Ma and D. Zhao, Chem. Soc. Rev., 2014, **43**, 4199.
4 C. W. Struijk, A. B. Sieval, J. E. J. Dakhorst, M. van Dijk, P. Kimkes, R. B. M. Koehorst, H. Donker, T. J. Schaafsma, S. J. Picken, A. M. van de Craats, J. M. Warman, H. Zuilhof and E. J. R. Sudho1lter, J. Am. Chem. Soc., 2000, **122**, 11057.
5 D. Veldman, S. C. J. Meskers and R. A. J. Janssen, Adv. Funct. Mater., 2009, **19**, 1939; W. Liu, R. Tkachov, H. Komber, V. Senkovskyy, M. Schubert, Z. Wei, A. Facchetti, D. Neher and A. Kiriy, Polymer Chem., 2014, **00**, 1.
6 E. Yang, J. Wang, J. R. Diers, D. M. Niedzwiedzki, C. Kirmaier, D. F. Bocian, J. S. Lindsey and D. Holten. J. Phys. Chem. B, 2014, **118**, 1630; K. M. Lefler, C. H. Kim, Y.-L. Wu and M. R. Wasielewski, J. Phys. Chem. Lett., 2014, **5**, 1608.
7 R. Shivanna, S. Shoaee, S. Dimitrov, S. K. Kandappa, S. Rajaram, J. R. Durrant and K. S. Narayan, Energy Environ. Sci., 2014, 7, 435.
8 L. Cao, Y.-Z. Wang, J.-Q. Zhong, Y.-Y. Han, W.-H. Zhang, X.-J. Yu, F.-Q. Xu, D.-C. Qi and A. T. S. Wee, J. Phys. Chem. C, 2014, **118**, 4160.
9 J. Li, F. Dierschke, J. Wu, A. C. Grimsdale and K. Müllen. J. Mater. Chem., 2006, **16**, 96; M. Planells, F. J. Céspedes-Guirao, A. Forneli, Á. Sastre-Santos, F. Fernández-Lázaro and E. Palomares, J. Mater. Chem., 2008, **18**, 5802; L. Zhao, T. Ma, H. Bai, G. Lu, C. Li and G. Shi, Langmuir, 2008, **24**, 4380.
10 H. Langhals, A. Obermeier, Y. Floredo, A. Zanelli and L. Flamigni, Chem. Eur. J., 2009, **15**, 12733.
11 W. S. Shin, H.-H. Jeong, M.-K. Kim, S.-H. Jin, M.-R. Kim, J.-K. Lee, J. W. Leec and Y.-S. Gal, J. Mater. Chem., 2006, **16**, 384.
12 A. Keerthi, Y. Liu, Q. Wang and S. Valiyaveettil, Chem. Eur. J., 2012, **18**, 11669; S. Mathew and H. Imahori, J. Mater. Chem., 2011, **21**, 7166.
13 F. Würthner, Chem. Commun., 2004, 1564; L. Schmidt-Mende, A. Fechtenkötter, K. Müllen, E. Moons, R. H. Friend and J. D. MacKenzie, Science, 2001, **293**, 1119.
14 I. M. Blake, L. H. Rees, T. D. W. Claridge and H. L. Anderson, Angew. Chem., Int. Ed., 2000, **39**, 1818; W. Zeng, B. S. Lee, Y. M. Sung, K.-W. Huang, Y. Li, D. Kim and J. Wu, Chem. Commun., 2012, **48**, 7684.
15 S. Chai, S.-H. Wen and K.-L. Han, Organic Electronics, 2011, **12**, 1806; J. Gao, C. Xiao, W. Jiang and Z. Wang, Org. Lett., 2014, **16**, 394.
16 A. D. Becke, J. Chem. Phys., 1993, **98**, 5648.
17 M. J. Frisch, G. W. Trucks, H. B. Schlegel and et al. Gaussian 03, revision C.02, Gaussian, Inc.: Wallingford, CT, 2004.
18 F. Würthner, V. Stepanenko, Z. Chen, C. R. Saha-Möller, N. Kocher and D. Stalke, J. Org. Chem., 2004, **69**, 7933.
19 A. A. Vasilev, K. D. Mey, I. Asselberghs, K. Clays, B. Champagne, S. E. Angelova, M. I. Spassova, C. Li and K. Müllen, J. Phys. Chem. C, 2012, **116**, 22711.
20 C.-C. Chao and M.-k. Leung, J. Org. Chem., 2005, **70**, 4323.
21 Á. J. Jiménez, M.-J. Lin, C. Burschka, J. Becker, V. Settels, B. Engels and F. Würthner, Chem. Sci., 2014, **5**, 608.
22 S. Vajiravelu, L. Ramunas, G. J. Vidas, G. Valentas, J. Vygintasc and S. Valiyaveettil, J. Mater. Chem., 2009, **19**, 4268.
23 Y. Zhu, A. R. Rabindranath, T. Beyerlein and B. Tieke, Macromolecules, 2007, **40**, 6981.
24 F. Würthner, C. Thalacker, S. Diele and C. Tschierske, Chem. Eur. J., 2001, **7**, 2245.
25 H. Langhals, S. Demmig and T. Potrawa, J. Prakt. Chem., 1991, **333**, 733; C. Burgdorff and H.-G. Löhmannsröben, Chem. Phys. Lett., 1992, **197**, 358.
26 A. D. Shaller, W. Wang, H. Gan and A. D. Q. Li, Angew. Chem., 2008, **120**, 7819; P. Osswald and F. Würthner, J. Am. Chem. Soc., 2007, **129**, 14319.
27 U. B. Cappel, M. H. Karlsson, N. G. Pschirer, F. Eickemeyer, J. Schöneboom, P. Erk, G. Boschloo and A. Hagfeldt, J. Phys. Chem. C, 2009, **113**, 14595.
28 Y. Li, Z. Pan, Y. Fu, Y. Chen, Z. Xie and B. Zhang, J. Polym. Sci., Part A: Polym. Chem., 2012, **50**, 1663.
29 Y. Li, J. Zou, H.-L. Yip, C.-Z. Li, Y. Zhang, C.-C. Chueh, J. Intemann, Y. Xu, P.-W. Liang, Y. Chen and A. K.-Y. Jen. Macromolecules, 2013, **46**, 5497.
30 S. Chen, Y. Liu, W. Qiu, X. Sun, Y. Ma and D. Zhu, Chem. Mater., 2005, **17**, 2208.
31 H. Zhen, K. Li, Z. Huang, Z. Tang, R. Wu, G. Li, X. Liu and F. Zhang, Appl. Phys. Lett., 2012, **100**, 213901.
32 G. Li, V. Shrotriya, J. Huang, Y. Yao, T. Moriarty, K. Emery and Y. Yang, Nat. Mater., 2005, **4**, 864.
33 X. Zhan, Z. Tan, B. Domercq, Z. An, X. Zhang, S. Barlow, Y. Li, D. Zhu, B. Kippelen and S. R. Marder, J. Am. Chem. Soc., 2007, **129**, 7246.
34 G. Dennler, M. C. Scharber and C. J. Brabec, Adv. Mater., 2009, **21**, 1323.
35 M. C. Scharber, D. Mühlbacher, M. Koppe, P. Denk, C. Waldauf, A. J. Heeger and C. J. Brabec, Adv. Mater., 2006, **18**, 789.
36 Y. Zou, D. Gendron, R. Badrou-Aïch, A. Najari, Y. Tao and M. Leclerc, Macromolecules, 2009, **42**, 2891.

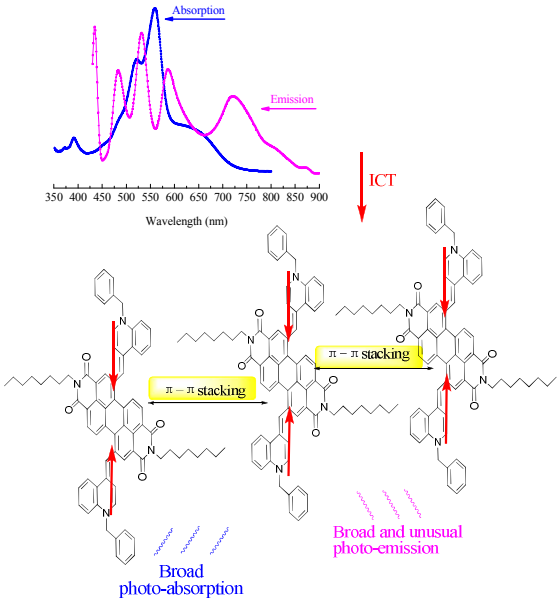

A simple synthetic route was applied to get perylene diimide derivatives with large conjugated system. Owing the extended π conjugated delocalization, the derivatives exhibit obvious intra-molecular charge transfer, broad photo-absorption and emission, concentration-dependant π-π staking induced fluorescence emission and low-lying LUMO energy level. The properties and analysis reveal that the derivatives are potential candidate materials in the areas of photovoltaic devices and photocatalyst.